

www.acsmaterialsletters.org

Lotus-Like Water Repellency of Gas-Phase-Synthesized Graphene

M. Weston Miller, Makenna Parkinson, and Albert Dato*



Cite This: ACS Materials Lett. 2022, 4, 995–1002



Read Online

ACCESS

Metrics & More

Article Recommendations

Supporting Information

ABSTRACT: The ability of lotus leaves to repel water is desired in numerous applications, such as self-cleaning surfaces, biomedical devices, and naval vessels. Creating materials that mimic the hierarchical structure and surface chemistry of lotus leaves requires multistep processes that are impractical for the mass production of nonwettable products. Superhydrophobic surfaces have been created using graphene. However, graphene sheets obtained through graphite exfoliation or deposition on substrates are not superhydrophobic and require additional processes to achieve lotus-like water repellency. In this work, we show that graphene produced in the gas phase is inherently superhydrophobic. Gas-phase-synthesized graphene (GSG) and lotus leaves have fundamentally different structures, yet water droplets on both materials

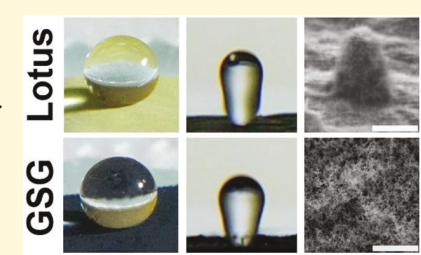


exhibit comparable contact angles, roll-off angles, and bouncing characteristics. Furthermore, hydrophilic surfaces become superhydrophobic when covered with GSG. The substrate-free synthesis of GSG is straightforward and sustainable, which could enable the manufacturing of a diverse range of water-repellent technologies.

ater droplets that impact the surface of a lotus leaf maintain a spherical shape after contact (Figure 1a) and roll off the natural material under the slightest gravitational force. 1,2 This phenomenon is called the Lotus Effect. 1-5 The water repellency of a lotus leaf is the result of a combination of (1) a hierarchical structure with micro- and nanoscale roughness and (2) a surface that has a low-surfaceenergy chemistry. 1,2,6 For example, scanning electron microscopy (SEM) images of the lotus leaf shown in Figure 1a reveal a surface that consists of microscale papillose epidermal cells (Figure 1b) that are coated with nanoscale epicuticular wax crystals (Figure 1c).^{2,3,7} Water maintains a Cassie state on top of lotus leaves because droplets make contact only with the tips of the wax crystals, which have a low surface energy.^{2,8} Water droplets that were deposited on the lotus leaf shown in Figure 1a were observed to have an average contact angle of 153.0 $^{\circ}$ \pm 2.0° (Figure 1d). Additionally, water droplets began to move on the surface of the lotus leaf at an average roll-off angle of $3.0^{\circ} \pm 0.6^{\circ}$ (Figure 1e and Movie S1 in the Supporting Information). Natural and artificial surfaces that have water contact angles greater than 150° and roll-off angles less than 10° are considered superhydrophobic.6

Creating artificial superhydrophobic surfaces is a challenge. Mimicking the hierarchical structure and surface chemistry of a lotus leaf is a strategy that has been used to achieve the Lotus Effect in artificial materials. ^{2,3,5,6,8,9} For instance, lotus-like surfaces have been created by patterning microstructures on hydrophilic surfaces and subsequently applying hydrophobic materials on the surfaces of the microstructures. ^{2,3,5} Consid-

erable attention has been placed on creating superhydrophobic surfaces using graphene, which is a single layer of sp^2 -bonded carbon atoms. ^{10,11} Contact angles ranging from 89.0° to 103.0° have been observed on flat graphene monolayers grown on substrates, 7,12,13 while contact angles as high as 137.3° were measured for water droplets on graphene nanowalls that were vertically grown on flat silicon substrates. 4,14,15 Contact angles between 120.0° to 130.0° have been reported for graphene powders produced through graphite exfoliation methods.7 However, achieving the Lotus Effect using graphene grown on substrates or obtained through the exfoliation of graphite requires additional processing steps, such as crumpling graphene sheets, 7,12,13 binding hydrophobic groups to graphene, incorporating graphene into polymers, has plasma surface treatments, soft-lithographic duplication, or growing graphene vertically on micropatterned pillars.⁴ The largescale manufacturing of a wide range of nonwettable applications through biomimicry or modified graphene is neither practical nor sustainable. The mass production of technologies that exhibit superhydrophobicity requires a material that is (1) inherently superhydrophobic and (2) simple and sustainable to create.

Received: February 9, 2022 Accepted: April 19, 2022



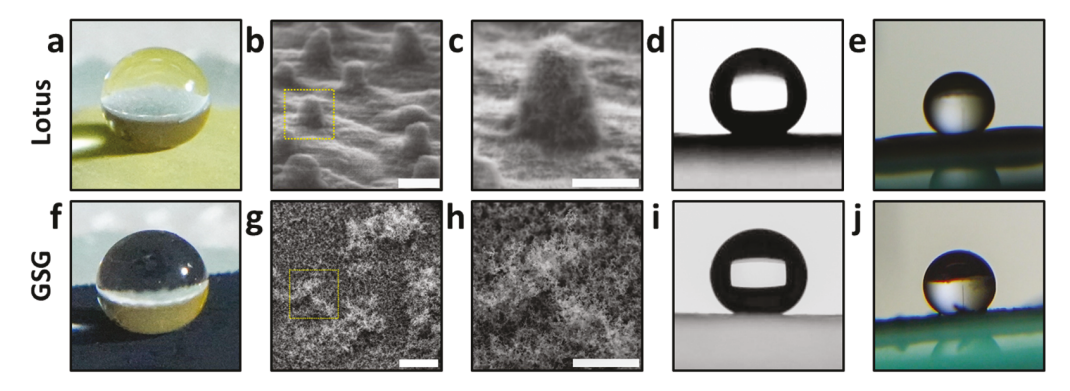


Figure 1. (a) Photograph of a water droplet on a lotus (Nelumbo nucifera) leaf. (b) SEM image of the papillose epidermal cells on the lotus leaf that impart a microscale roughness on its surface. Scale bar is $10 \, \mu \text{m}$. (c) SEM image of the single epidermal cell taken from the region indicated by the yellow box in (b). The epicuticular wax crystals on the surface of the cell give it a nanoscale roughness and a fuzzy appearance. Scale bar is $5 \, \mu \text{m}$. (d) Photograph showing the contact angle of a water droplet on a lotus leaf. The average contact angle of water droplets on the lotus leaf was $153.0^{\circ} \pm 2.0^{\circ}$. (e) Photograph of a water droplet taken immediately prior to rolling off the surface of the lotus leaf. This is a video frame from Movie S1 in the Supporting Information. The average roll-off angle for water droplets on the lotus leaf was $3.0^{\circ} \pm 0.6^{\circ}$. (f) Photograph of a water droplet on as-synthesized and unmodified GSG collected on a nylon filter. (g) SEM image of the surface of the GSG specimen. Scale bar is $10 \, \mu \text{m}$. (h) SEM image taken from the region indicated by the yellow box in (g) that shows the porous and cloud-like GSG powder. Scale bar is $5 \, \mu \text{m}$. (i) Photograph showing the contact angle of a water droplet on GSG. The average contact angle of water droplets on GSG specimens was $153.0^{\circ} \pm 3.0^{\circ}$. (j) Photograph of a water droplet taken immediately prior to rolling off the surface of the GSG specimen. The average roll-off angle of water droplets on GSG specimens was $4.8^{\circ} \pm 1.1^{\circ}$. This is a video frame from Movie S1 in the Supporting Information.

Graphene can be synthesized without substrates in a single step by delivering ethanol into an atmospheric-pressure microwave-generated argon plasma. $^{18-20}$ The dissociation of ethanol in an atmospheric argon plasma produces reactive fragments that rapidly form graphene sheets, which are collected downstream from the plasma. 18 The main byproducts of the substrate-free gas-phase synthesis process are CO and H2, which can be used to create fuels and other industrial chemicals.¹⁹ Gas-phase-synthesized graphene (GSG) consists of highly ordered single-layer, bilayer, and few-layered graphene sheets that have a mass composition of 98.9% C, 1.0% H, and 0.1% O. 19,20 The high quality of GSG 20 has enabled the transmission electron microscopy (TEM) imaging of soft-hard interfaces on nanomaterials, 21 enhanced the mechanical properties of polymer-matrix nanocomposites, 22 and improved the lubricating properties of motor oils.²³ Here, we demonstrate that as-synthesized and unmodified GSG is inherently superhydrophobic.

The lotus-like water repellency of GSG was discovered when water droplets were deposited directly onto GSG that was collected on nylon filters (Figure 1f). A low-magnification SEM image of the GSG powder on a nylon filter is shown in Figure 1g and a higher magnification SEM image of GSG is shown in Figure 1h. The SEM images reveal the porous and cloud-like structure of GSG, which is completely different from the surface structure of a lotus leaf. Remarkably, water droplets on GSG exhibit an average contact angle of $153.0^{\circ} \pm 3.0^{\circ}$ (Figure 1i), which is equivalent to the average contact angle that was observed on the lotus specimen (Figure 1d). As shown in Figure 1j and Movie S1 in the Supporting Information, static water droplets began to move on the GSG surface at an average roll-off angle of $4.8^{\circ} \pm 1.1^{\circ}$, which is very close to the average roll-off angle of the lotus leaf (Figure 1e). The similarities in contact angles and roll-off angles between GSG and the lotus leaf are surprising because of the fundamentally different structures and compositions of the two materials.

GSG and lotus leaves also repel free-falling water droplets in a comparable manner. Water droplets with a diameter of 2 mm were released at a height of 15 mm above a lotus leaf and GSG, which resulted in an impact velocity of 0.4 m/s. A high-speed video camera was used to record changes in the shapes of water droplets impacting the two specimens. Figure 2a and Movie S2 in the Supporting Information clearly show that water droplets impacted, deformed, retracted, and rebounded from GSG and the lotus leaf in the same way. Figure 2b and Movie S3 in the Supporting Information show that the deformation and bouncing of water droplets on GSG and the lotus leaf were also nearly identical at a higher droplet release height of 70 mm, which corresponded to an impact velocity of 1.1 m/s. Water droplets that fall on lotus leaves experience significant changes in shape during impact as the kinetic energy of the droplets transforms into stored energy due to surface deformation.² Furthermore, the elasticity of water droplets on lotus leaves arises from the efficient interchange between kinetic energy and surface energy during droplet deformation.² The results indicate that water droplets experienced similar transformations and interchanges of energy on both GSG and the lotus leaf. For both the 15 and 70 mm release heights, droplets on both GSG and the lotus leaf maintained a spherical shape upon coming to rest. Water droplets that settle on lotus leaves effectively form a composite solid-air-liquid interface and retain high contact angles, 3,9 and the results suggest that water droplets form a comparable solid-air-liquid interface on GSG.

The impalement of water droplets falling on the bare nylon filters used for collecting GSG indicate that the graphene powder is inherently superhydrophobic. As shown in Movie S4 and Figure S1 in the Supporting Information, a water droplet that was released from a height of 70 mm immediately stuck to a nylon filter upon impact. Furthermore, the droplet did not form a spherical shape and had a contact angle below 90° after it settled on the nylon surface. This result indicates that the superhydrophobicity of GSG on nylon was strictly due to the interaction of water with GSG.

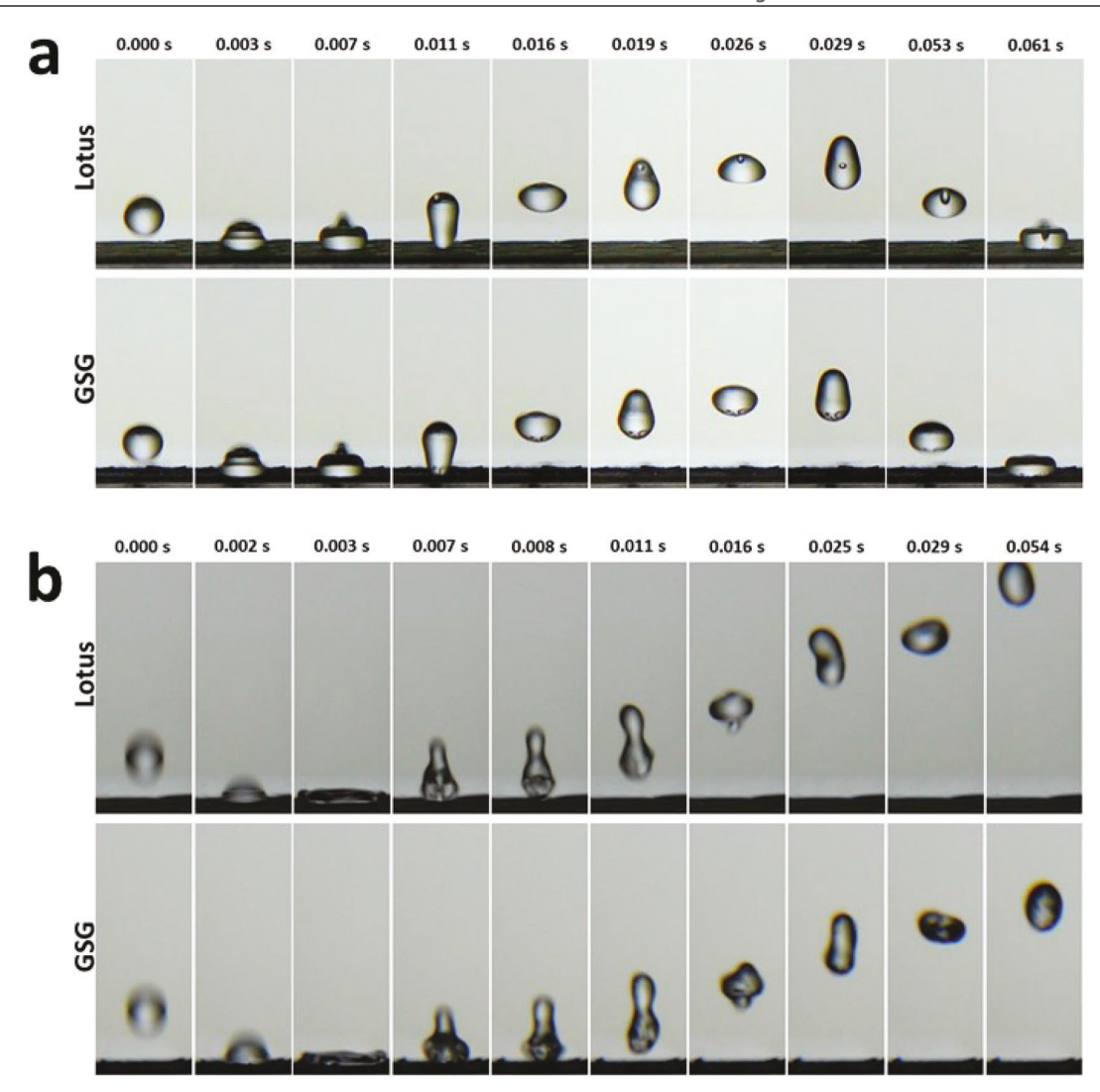


Figure 2. (a) Snapshots from Movie S2 in the Supporting Information that show water droplets experiencing similar rebounds and changes in shape when impacting a lotus leaf and GSG at 0.4 m/s. (b) Snapshots from Movie S3 in the Supporting Information that show water droplets experiencing similar rebounds and changes in shape when impacting a lotus leaf and GSG at 1.1 m/s.

The water repellency of other hydrophilic surfaces covered with GSG further demonstrate the nonwettability of the nanomaterial. Movie S5 and Figure S1 in the Supporting Information show that a water droplet falling on a hydrophilic aluminum specimen easily adhered to the metal surface and had a contact angle below 90°. Covering aluminum with GSG drastically increased the average contact angle of water to $159.6^{\circ} \pm 2.7^{\circ}$ (Figure 3a). Furthermore, the presence of GSG on aluminum resulted in an average roll-off angle of 7.7° \pm 3.3°. Figure 3b and Movie S5 in the Supporting Information show that a water droplet bouncing on GSG-covered aluminum resembles the bouncing of water droplets on the lotus leaf specimen. In another experiment, water droplets impacting a flat silicon wafer readily attached to the hydrophilic surface, which is shown in Movie S6 and Figure S1 in the Supporting Information. Silicon became superhydrophobic when GSG was deposited on its surface. As shown in Figure 3c and Movie S7 in the Supporting Information, the average contact angle and average roll-off angle of water droplets on GSG-covered silicon was measured to be $163.7^{\circ} \pm 2.3^{\circ}$ and $4.2^{\circ} \pm 1.2^{\circ}$, respectively. Figure 3d and Movie S6 in the Supporting Information demonstrate that

silicon covered with GSG also repelled water like the lotus leaf specimen. This initial study into the application of GSG as a water-repellent coating suggests that superhydrophobic surfaces could be created by applying GSG to hydrophilic materials.

Fabricating nonwettable surfaces using GSG will require methods of adhering the sheets to materials. The studies of GSG on nylon were conducted on powders that were captured on nylon membrane filters that were located downstream from atmospheric plasmas during the production of GSG. Silicon wafer specimens covered with GSG were created by mounting square pieces of silicon $(1.0 \times 1.0 \text{ cm})$ directly on the nylon filters using double-sided Scotch tape. GSG impacted the silicon pieces and adhered to the surfaces, which is a phenomenon that was previously reported in an in situ TEM study that directly observed the deformation behavior of individual GSG sheets being manipulated by a silicon probe.²⁴ Aluminum was covered with GSG by removing the powder from the nylon filters and depositing the nanomaterial directly on the metal. The results of the GSG on aluminum experiments were obtained from flakes that were at rest on the metal surfaces. Therefore, falling water droplets caused the

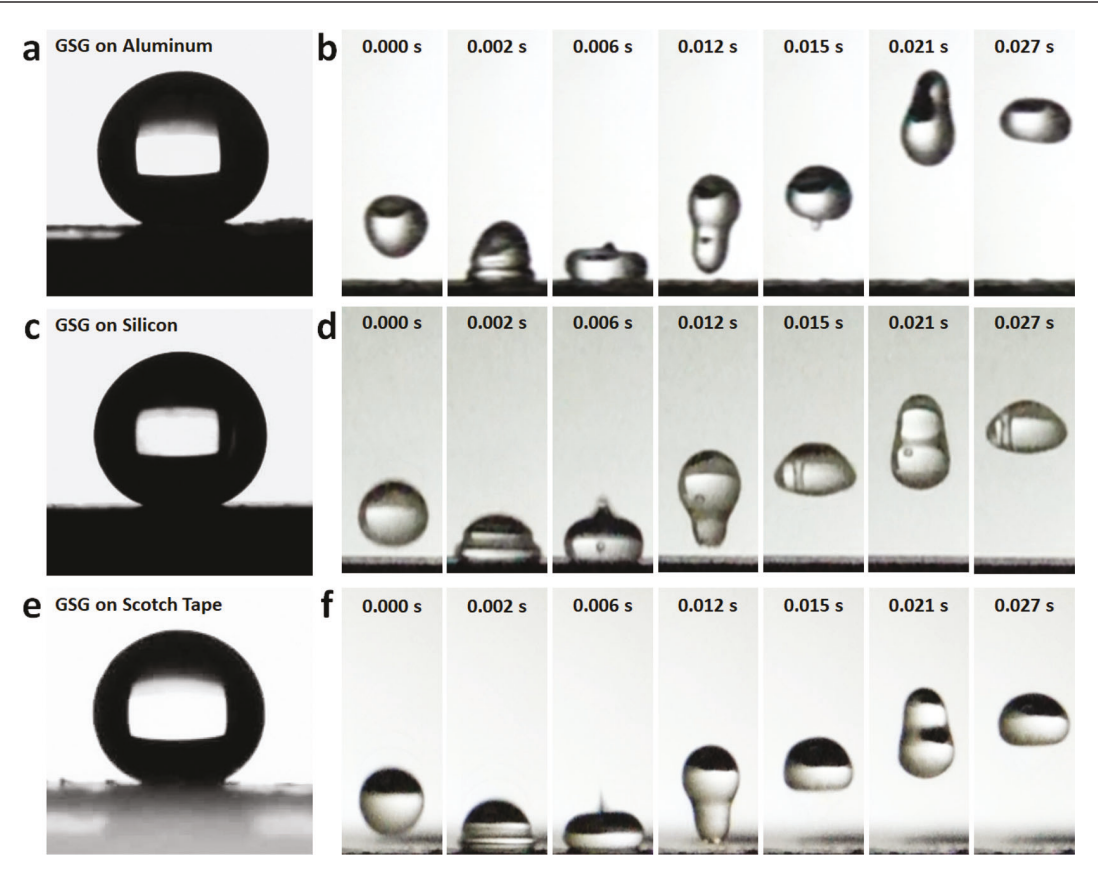


Figure 3. (a) Photograph of a water droplet on an aluminum surface covered with GSG. The average contact angle of water droplets on GSG-covered aluminum surfaces was $159.6^{\circ} \pm 2.7^{\circ}$. (b) Snapshots from Movie S5 that show the changes in shape and rebound of a water droplet falling on aluminum covered with GSG at an impact velocity of 0.4 m/s. (c) Photograph of a water droplet on silicon covered with GSG. The average contact angle of water on GSG-coated silicon was $163.7^{\circ} \pm 2.3^{\circ}$. (d) Snapshots from Movie S6 that show the initial bounce of a water droplet on silicon covered with GSG at an impact velocity of 0.4 m/s. (e) Photograph of a water droplet on GSG bound to Scotch tape. The average contact angle of water droplets on GSG attached to Scotch tape was $164.3^{\circ} \pm 2.7^{\circ}$. (f) Snapshots from Movie S8 that show a water droplet bouncing on GSG on Scotch tape at an impact velocity of 0.4 m/s.

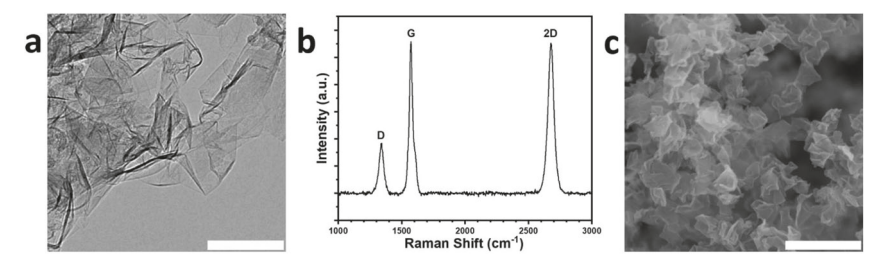


Figure 4. (a) TEM image of GSG that shows the submicron lateral dimensions of the atomically thin sheets. Scale bar is 100 nm. (b) Raman spectrum of GSG. (c) High-magnification SEM image of GSG that shows numerous sharp features and empty spaces that are present in GSG powder. Scale bar is 500 nm.

GSG flakes to easily detach from the underlying materials and attach to the surfaces of the droplets, which can be observed in Movies S1, S2, S3, S4, S5, S6, and Figure S2 in the Supporting Information. The use of binders to affix GSG to arbitrary surfaces is necessary to harnessing the superhydrophobicity of the nanomaterial.

The effect of a binder on the nonwettability of GSG was investigated by studying the interactions between water droplets and GSG attached to Scotch tape. Movie S8 and Figure S1 in the Supporting Information show that falling water droplets stuck to bare Scotch tape upon impact. Adhering GSG to Scotch tape instantly resulted in a superhydrophobic surface. Average contact angles of water

droplets on GSG attached to Scotch tape were $164.3^{\circ} \pm 2.7^{\circ}$ (Figure 3e), while the average roll-off angle of water droplets was measured to be $4.0^{\circ} \pm 2.0^{\circ}$, which is shown in Movie S7 in the Supporting Information. Importantly, Movie S8 in the Supporting Information and Figure 3f indicate that the adhesive on the Scotch tape did not diminish the ability of GSG to repel water droplets. Water droplets bounced from GSG on Scotch tape in a similar manner as the lotus leaf and GSG on nylon, silicon, and aluminum. Furthermore, water droplets falling on Scotch tape containing GSG had visibly less powder on their surfaces relative to water droplets impacting GSG on nylon, which is shown in Figure S2 in the Supporting Information. This result implies that the Scotch tape adhesive

alleviated the loss of powder when water impacted the GSG-covered tape. Therefore, these experiments suggest that the superhydrophobicity of GSG can persist even when the nanomaterial is affixed to a surface using a binder. Future research will investigate mechanically stable methods of adhering GSG to arbitrary materials to create robust water-repellent surfaces.

Electron microscopy and Raman spectroscopy of GSG indicate that the nanomaterial possesses a unique combination of features that could be simultaneously contributing to its water repellency. TEM imaging of GSG (Figure 4a) reveals that the powder consists of crumpled and randomly oriented sheets that are nearly transparent to an electron beam. Three prominent peaks are present in the Raman spectrum of GSG (Figure 4b): a D peak at \sim 1340 cm⁻¹, a G peak at \sim 1570 cm $^{-1}$, and a single sharp 2D peak at ~2680 cm $^{-1}$ that is characteristic of graphene. The intensity ratio of the 2D and G peaks (I_{2D}/I_G) is ~1.0 and the intensity ratio of the G and D peaks (I_G/I_D) is ~2.9, which shows that the GSG powder used in this study consisted of high-quality single-layer, bilayer, and few-layer graphene sheets. 10,11 The nonwettability of GSG is remarkable because graphene produced by other methods that exhibit morphologies or Raman spectra that are similar to GSG are not inherently superhydrophobic. For example, "carbon aerosols" that are produced through a different plasma-based process²⁵ resemble GSG but can only achieve a maximum contact angle of 141.0°. The intensity ratio of the 2D and G peaks in the Raman spectra of "carbon aerosols" was reported to be below unity $(I_{2D}/I_G \sim 0.7)^{25}$ which shows that "carbon aerosols" consist of multilayer graphene and graphite. Relative to "carbon aerosols", the Raman spectrum of GSG has a higher I_{2D}/I_{G} , which suggests that GSG sheets are thinner than "carbon aerosols". 11 Increasing the number of layers in a graphene sheet has been shown to decrease the contact angle of water droplets on the nanomaterial. 26,27 However, the thinness of GSG may not be the only factor contributing to its propensity to repel water. Graphene grown on silicon substrates by plasma enhanced chemical vapor deposition (CVD) using a tea tree extract as a precursor were reported to have an $I_{\rm 2D}/I_{\rm G}$ of ~3.3, which implies that the sheets consisted mainly of graphene with less than three atomic layers. 15 However, water droplets on graphene produced using the natural precursor had contact angles of only 135.0°. 15 Relative to graphene grown on silicon by plasma enhanced CVD, GSG on silicon achieved much higher contact angles despite having a lower $I_{\rm 2D}/I_{\rm G}$. In another study that investigated graphene grown on silicon substrates, few-layer graphene nanosheets created using microwave plasma CVD exhibited similar Raman peaks and peak intensity ratios as GSG but achieved a contact angle of only 132.9°.4 A chemical modification of the few-layer graphene nanosheets resulted in a marginal increase in contact angle to 133.7°. Superhydrophobicity was only attained when few-layer graphene nanosheets were grown on microfabricated silicon structures followed by the chemical modification. In contrast, as-synthesized GSG deposited on flat silicon wafers achieved lotus-like water repellency without silicon microstructures or chemical modification. On the basis of these results, other factors in GSG could be causing water droplets that fall on the nanomaterial to bounce and maintain their spherical shapes upon coming to rest.

The extremely crumpled nature and small lateral size of GSG could be enhancing its ability to repel water. The high-

magnification SEM image shown in Figure 4c reveals that GSG powder consists of graphene sheets that are not flat. Flat monolayer graphene is not superhydrophobic, 12,13,26,27 but a water contact angle of 152° was achieved on flat graphene that was synthesized on a nickel substrate by CVD, transferred to a polydimethylsiloxane stamp, and deliberately crumpled.¹³ The highly crumpled morphology of as-synthesized GSG could be causing the contact angles of water droplets on the powder to exceed 150°. Furthermore, carbon nanowalls, graphene grown on substrates, ^{7,12,13} and graphene obtained through the exfoliation of graphite ^{7,16,28} have micrometer-scale lateral dimensions and are not inherently superhydrophobic. In contrast, individual GSG sheets have submicron lateral dimensions (Figure 4a). Countless sheet edges, sheet corners, and empty spaces that can entrap air exist in GSG powder because of the substantial crumpling and small sizes of the flakes (Figure 4c). The multitude of sharp features on surfaces covered with GSG may be creating an effect that is akin to a bed of nails (Fakir state)^{8,29,30} that prevents the impalement of water droplets impacting the surfaces.

Factors that could also be contributing to the nonwettability of GSG include graphitic staples and other water-repelling mechanisms. GSG contains graphitic staples that maintain its crumpled morphology and enable the graphene sheets to reversibly deform without strain hardening.²⁴ Graphitic staples may be preventing GSG from flattening during water droplet impacts and enable the crumpled flakes to behave like springs, which could be contributing to the bouncing of water droplets on the GSG surface. Recently, the presence of water in motor oil was found to cause GSG to segregate in low-moisture regions of the fluid.²³ GSG dispersed homogeneously throughout the lubricant when moisture was removed through heating.²³ The mechanisms behind the tendency of GSG to avoid water when immersed in oil have yet to be determined, but these mechanisms may also be causing GSG to repel water in air. Future studies into the exact mechanisms of superhydrophobicity in GSG could result in methods of achieving nonwettability in other materials.

In summary, graphene produced through the substrate-free gas-phase synthesis method exhibits lotus-like water repellency. GSG requires no additional processes to achieve the Lotus Effect. Hydrophilic surfaces become superhydrophobic when covered with GSG. The mechanisms behind the inherent nonwettability of GSG require further research because a unique combination of features in the nanomaterial could be contributing to its ability to repel water. GSG can potentially provide a feasible pathway to the large-scale manufacturing of a broad range of superhydrophobic technologies, such as self-cleaning surfaces, oil—water separators, anti-icing applications, fluid transportation, drag-reducing coatings, and biomedical devices.

■ EXPERIMENTAL METHODS

The graphene used in this study was prepared by the substrate-free gas-phase synthesis method. Aerosols consisting of ethanol droplets and argon gas were delivered directly into atmospheric-pressure microwave-generated argon plasmas. The plasmas were generated at an applied microwave forward power of 250 W. The microwave plasma reactor used to produce graphene was a commercially available MKS/ASTeX AX2518 system. Argon plasmas were ignited and sustained using an argon flow rate of 2.0 L/min into the reactor. The flow rate of ethanol and argon in the aerosol was 0.3 and 3.0

L/min, respectively. GSG was collected downstream from the plasma on nylon filters (Nylaflo Membrane Disc Filter 28140-042).

Lotus (Nelumbo nucifera) leaves, nylon filters containing GSG, and bare nylon filters were mounted on standard glass slides $(2.5 \times 7.5 \text{ cm})$ using double-sided Scotch tape. Dry and unmodified GSG powder was gently removed from nylon filters and deposited directly on aluminum SEM stubs (Ted Pella Product #16111). Silicon specimens containing GSG were prepared by mounting square silicon pieces (1.0×1.0) cm) directly onto nylon membrane filters using double-sided 3M Scotch tape. The filters with silicon pieces were then mounted downstream from the plasma reactor during the production of GSG. Silicon wafers containing GSG were analyzed using Raman spectroscopy. Scotch tape containing GSG was prepared by mounting double-sided 3M Scotch tape on standard glass slides. GSG was adhered to the tape by pressing the slides against the GSG powder on the nylon filters. SEM specimens were prepared by mounting lotus leaves and nylon filters containing GSG onto aluminum SEM stubs using electrically conductive double-sided tape (3M Z Axis Tape). TEM specimens were prepared by dispersing GSG in ethanol and depositing a droplet of the dispersion on a lacey carbon TEM grid. Ethanol was evaporated from the grid prior to TEM imaging.

Contact angle measurements were conducted using an Ossila Contact Angle Goniometer Model L2004A1. Side-byside measurements of contact angles on lotus leaves and GSG on nylon were performed by depositing 5 μ L water droplets on the specimens at ambient conditions. Videos and images of water droplets on the specimens (Figure 1d,i) were taken using the camera on the L2004A1, which captured videos at a resolution of 1920 × 1080 at 30 frames per second. Ossila Contact Angle Software was used to determine the contact angle of water droplets on specimens. Average contact angle values and standard deviations were determined from 30 separate measurements of water droplets on GSG specimens and 10 separate measurements of water droplets on lotus specimens. This procedure was also performed on water droplets deposited on aluminum SEM stubs covered with GSG (Figure 3a), GSG on silicon (Figure 3c), and Scotch tape containing GSG (Figure 3e). Average contact angle values and standard deviations were determined from 20 separate measurements of water droplets on GSG-covered aluminum SEM stubs, 10 separate measurements of water droplets on GSG-covered silicon, and 10 separate measurements of water droplets on GSG-covered Scotch tape.

Roll-off angle measurements were determined by placing the specimens on a single-axis goniometric stage. Droplets with a volume of 5 μ L were deposited on the specimens at ambient conditions and were allowed to come to rest. The goniometric stage was slowly rotated until droplets rolled off the specimens. Movies S1 and S7 were obtained using a Sony ZV-1 camera that recorded videos at a resolution of 1920 \times 1080 at 60 frames per second. The camera was used to record the roll-off angle experiments and capture the exact moment that droplets rolled off each specimen. Average roll-off angle values and standard deviations were determined from 30 separate measurements of water droplets rolling off GSG specimens and 10 separate measurements of water droplets rolling off lotus specimens. This procedure was also performed on water droplets deposited on aluminum SEM stubs covered with GSG, GSG-coated silicon, and Scotch tape containing GSG.

Average roll-off angle values and standard deviations were determined from 15 separate measurements of water droplets on the GSG-covered aluminum SEM stubs, 10 separate measurements of water droplets on GSG on silicon, and 10 separate measurements of water droplets on GSG-covered Scotch tape.

For droplet impact tests, specimens were placed directly beneath a microliter syringe that dispensed 5 μ L water droplets on the specimens. The tip of the syringe was located at 15 and 70 mm above the centers of the specimens during experiments. High-speed camera videos of droplet impacts (Movies S2, S3, S4, S5, S6, and S8) were taken using a Sony ZV-1 camera that recorded at a resolution of 1920 \times 1080 at 960 frames per second. Images of droplet impacts (Figures 2a,b, 3b,d,f, and S1) were obtained from frames of the high-speed camera videos.

Raman spectroscopy was performed on GSG-covered silicon specimens using a laser with a wavelength of 532 nm (Figure 4b). SEM images of GSG and a lotus leaf (Figure 1b,c,g,h) were taken using a ThermoFisher Scientific Quanta 3D 200i. The high-magnification SEM image of GSG (Figure 4c) was taken using a ThermoFisher Scientific NNS450. Both microscopes are located at the Central Facility for Advanced Microscopy and Microanalysis at UC Riverside. The TEM image shown in Figure 4a was taken using a 120 kV Tecnai12 at the Central Facility for Advanced Microscopy and Microanalysis at UC Riverside.

ASSOCIATED CONTENT

Supporting Information

The Supporting Information is available free of charge at https://pubs.acs.org/doi/10.1021/acsmaterialslett.2c00125.

High-speed camera images of water droplets falling on four surfaces: a nylon filter, an aluminum SEM stub, a silicon wafer, and Scotch tape; Images comparing the residues on water droplets bouncing from a lotus leaf, GSG on nylon, and GSG on Scotch tape (PDF)

Movie S1 - Video that demonstrates the comparable roll-off angles of water droplets on lotus leaves and GSG (MP4) (MP4)

Movie S2 — High-speed camera video that shows water droplets experiencing similar rebounds and changes in shape when impacting a lotus leaf and GSG at 0.4 m/s (MP4)

Movie S3 — High-speed camera video that shows water droplets experiencing similar rebounds and changes in shape when impacting a lotus leaf and GSG at 1.1 m/s (MP4)

Movie S4 – High-speed camera video that shows the high adhesion of water to a bare nylon filter (MP4)

Movie S5 – High-speed camera video that shows the impacts of water droplets falling on an aluminum surface covered with GSG and a bare aluminum surface at an impact velocity of 0.4 m/s (MP4)

Movie S6 – High-speed camera video that shows the impacts of water droplets falling on silicon covered with GSG and a bare silicon surface at an impact velocity of 0.4 m/s (MP4)

Movie S7 — Video that demonstrates the low roll-off angles of water droplets on GSG on silicon and GSG on Scotch tape (MP4)

Movie S8 – High-speed camera video that shows the impacts of water droplets falling on GSG attached to Scotch tape and bare Scotch tape at an impact velocity of 0.4 m/s (MP4)

AUTHOR INFORMATION

Corresponding Author

Albert Dato — Department of Engineering, Harvey Mudd College, Claremont, California 91711, United States; orcid.org/0000-0001-9902-5977; Email: adato@ hmc.edu

Authors

M. Weston Miller – Department of Engineering, Harvey Mudd College, Claremont, California 91711, United States Makenna Parkinson – Department of Engineering, Harvey Mudd College, Claremont, California 91711, United States

Complete contact information is available at: https://pubs.acs.org/10.1021/acsmaterialslett.2c00125

Author Contributions

The paper was written through contributions of all authors. A.D. was the principal investigator who conceived and supervised the research. M.W.M. and M.P. performed the experiments and obtained the data. All authors analyzed the data. A.D. obtained the SEM and TEM images. A.D. wrote the paper and prepared the figures and videos. All authors have given approval to the final version of the paper.

Notes

The authors declare no competing financial interest.

■ ACKNOWLEDGMENTS

This study was supported by the National Science Foundation under Grant No. 1943599. This study was also supported by the Harvey Mudd College Rasmussen Summer Research Fund. Transmission electron microscopy and scanning electron microscopy imaging were performed at the Central Facility for Advanced Microscopy and Microanalysis at UC Riverside. We thank Mystic Koi & Water Gardens in Claremont, California and Van Ness Water Gardens in San Antonio Heights, California for donating the lotus leaves used in this work.

REFERENCES

- (1) Marmur, A. Super-hydrophobicity fundamentals: implications to biofouling prevention. *Biofouling* **2006**, 22 (1–2), 107–115.
- (2) Zorba, V.; Stratakis, E.; Barberoglou, M.; Spanakis, E.; Tzanetakis, P.; Anastasiadis, S. H.; Fotakis, C. Biomimetic Artificial Surfaces Quantitatively Reproduce the Water Repellency of a Lotus Leaf. *Adv. Mater.* **2008**, *20* (21), 4049–4054.
- (3) Bhushan, B.; Jung, Y. C. Natural and biomimetic artificial surfaces for superhydrophobicity, self-cleaning, low adhesion, and drag reduction. *Prog. Mater. Sci.* **2011**, *56* (1), 1–108.
- (4) Dong, J.; Yao, Z. H.; Yang, T. Z.; Jiang, L. L.; Shen, C. M. Control of Superhydrophilic and Superhydrophobic Graphene Interface. Sci. Rep. 2013, 3, 6.
- (5) Long, J.; Fan, P.; Gong, D.; Jiang, D.; Zhang, H.; Li, L.; Zhong, M. Superhydrophobic surfaces fabricated by femtosecond laser with tunable water adhesion: from lotus leaf to rose petal. *ACS Appl. Mater. Interfaces* **2015**, *7* (18), 9858–9865.
- (6) Wang, D.; Sun, Q.; Hokkanen, M. J.; Zhang, C.; Lin, F. Y.; Liu, Q.; Zhu, S. P.; Zhou, T.; Chang, Q.; He, B.; Zhou, Q.; Chen, L.; Wang, Z.; Ras, R. H. A.; Deng, X. Design of robust superhydrophobic surfaces. *Nature* **2020**, *582* (7810), 55–59.

- (7) Wang, J. N.; Zhang, Y. L.; Liu, Y.; Zheng, W.; Lee, L. P.; Sun, H. B. Recent developments in superhydrophobic graphene and graphene-related materials: from preparation to potential applications. *Nanoscale* **2015**, *7* (16), 7101–7114.
- (8) Papadopoulos, P.; Mammen, L.; Deng, X.; Vollmer, D.; Butt, H. J. How superhydrophobicity breaks down. *Proc. Natl. Acad. Sci. U. S. A.* **2013**, *110* (9), 3254–3258.
- (9) Jung, Y. C.; Bhushan, B. Dynamic effects of bouncing water droplets on superhydrophobic surfaces. *Langmuir* **2008**, 24 (12), 6262–6269.
- (10) Malard, L. M.; Pimenta, M. A.; Dresselhaus, G.; Dresselhaus, M. S. Raman spectroscopy in graphene. *Phys. Rep.* **2009**, 473 (5–6), 51–87.
- (11) Ferrari, A. C.; Meyer, J. C.; Scardaci, V.; Casiraghi, C.; Lazzeri, M.; Mauri, F.; Piscanec, S.; Jiang, D.; Novoselov, K. S.; Roth, S.; Geim, A. K. Raman spectrum of graphene and graphene layers. *Phys. Rev. Lett.* **2006**, *97* (18), 187401.
- (12) Chen, Z. X.; Dong, L.; Yang, D.; Lu, H. B. Superhydrophobic Graphene-Based Materials: Surface Construction and Functional Applications. *Adv. Mater.* **2013**, 25 (37), 5352–5359.
- (13) Zang, J. F.; Ryu, S.; Pugno, N.; Wang, Q. M.; Tu, Q.; Buehler, M. J.; Zhao, X. H. Multifunctionality and control of the crumpling and unfolding of large-area graphene. *Nat. Mater.* **2013**, *12* (4), 321–325.
- (14) Watanabe, H.; Kondo, H.; Sekine, M.; Hiramatsu, M.; Hori, M. Control of Super Hydrophobic and Super Hydrophilic Surfaces of Carbon Nanowalls Using Atmospheric Pressure Plasma Treatments. *Jpn. J. Appl. Phys.* **2012**, *51* (1), 01AJ07.
- (15) Jacob, M. V.; Rawat, R. S.; Ouyang, B.; Bazaka, K.; Kumar, D. S.; Taguchi, D.; Iwamoto, M.; Neupane, R.; Varghese, O. K. Catalyst-Free Plasma Enhanced Growth of Graphene from Sustainable Sources. *Nano Lett.* **2015**, *15* (9), 5702–5708.
- (16) Asthana, A.; Maitra, T.; Buchel, R.; Tiwari, M. K.; Poulikakos, D. Multifunctional superhydrophobic polymer/carbon nanocomposites: graphene, carbon nanotubes, or carbon black? *ACS Appl. Mater. Interfaces* **2014**, *6* (11), 8859–8867.
- (17) Yun, X.; Xiong, Z.; He, Y.; Wang, X. Superhydrophobic lotus-leaf-like surface made from reduced graphene oxide through soft-lithographic duplication. *Rsc Adv.* **2020**, *10* (9), 5478–5486.
- (18) Dato, A.; Radmilovic, V.; Lee, Z.; Phillips, J.; Frenklach, M. Substrate-free gas-phase synthesis of graphene sheets. *Nano Lett.* **2008**, 8 (7), 2012–2016.
- (19) Dato, A. Graphene synthesized in atmospheric plasmas—A review. J. Mater. Res. 2019, 34 (1), 214–230.
- (20) Dato, A.; Lee, Z.; Jeon, K. J.; Erni, R.; Radmilovic, V.; Richardson, T. J.; Frenklach, M. Clean and highly ordered graphene synthesized in the gas phase. *Chem. Commun.* (*Camb*) **2009**, 40, 6095–6097.
- (21) Lee, Z.; Jeon, K. J.; Dato, A.; Erni, R.; Richardson, T. J.; Frenklach, M.; Radmilovic, V. Direct imaging of soft-hard interfaces enabled by graphene. *Nano Lett.* **2009**, *9* (9), 3365–3369.
- (22) Nakahara, K.; Knego, J.; Sloop, T.; Bisquera, C.; Subler, N.; Dato, A. Enhanced mechanical properties of epoxy-matrix nanocomposites reinforced with graphene synthesized in atmospheric plasmas. *Plasma Processes and Polymers* **2020**, *17* (5), 1900244.
- (23) Krauss, G. G.; Dato, A.; Siniawski, M. Enhanced lubricating properties of oils containing graphene synthesized in atmospheric plasmas. *Carbon Trends* **2020**, *1*, 100010.
- (24) Lin, A. Y. W.; Yu, X.-x.; Dato, A.; Krauss, G.; Marks, L. D. In situ observations of graphitic staples in crumpled graphene. *Carbon* **2018**, *132*, 760–765.
- (25) Wu, A. J.; Li, X. D.; Yang, J.; Yan, J. H. Synthesis and characterization of a plasma carbon aerosol coated sponge for recyclable and efficient separation and adsorption. *Rsc Adv.* **2017**, *7* (15) 9303–9308
- (26) Taherian, F.; Marcon, V.; van der Vegt, N. F.; Leroy, F. What is the contact angle of water on graphene? *Langmuir* **2013**, 29 (5), 1457–1465.

- (27) Shih, C. J.; Wang, Q. H.; Lin, S.; Park, K. C.; Jin, Z.; Strano, M. S.; Blankschtein, D. Breakdown in the wetting transparency of graphene. *Phys. Rev. Lett.* **2012**, *109* (17), 176101.
- (28) Rafiee, J.; Rafiee, M. A.; Yu, Z. Z.; Koratkar, N. Superhydrophobic to Superhydrophilic Wetting Control in Graphene Films. *Adv. Mater.* **2010**, 22 (19), 2151–2154.
- (29) Maitra, T.; Tiwari, M. K.; Antonini, C.; Schoch, P.; Jung, S.; Eberle, P.; Poulikakos, D. On the Nanoengineering of Superhydrophobic and Impalement Resistant Surface Textures below the Freezing Temperature. *Nano Lett.* **2014**, *14* (1), 172–182.
- (30) Shirtcliffe, N. J.; McHale, G.; Atherton, S.; Newton, M. I. An introduction to superhydrophobicity. *Adv. Colloid Interface Sci.* **2010**, 161 (1-2), 124-138.